DOI: 10.1002/anie.201108276

P-Doped Photocatalysts

Phosphate Doping into Monoclinic $BiVO_4$ for Enhanced Photoelectrochemical Water Oxidation Activity**

*Won Jun Jo, Ji-Wook Jang, Ki-jeong Kong, Hyun Joon Kang, Jae Young Kim, Hwichan Jun, K. P. S. Parmar, and Jae Sung Lee**

Hydrogen has been touted as an energy carrier of the future because it combines with oxygen to produce only water with no greenhouse gases or other pollutants. For hydrogen to play the role, it must be produced in a sustainable manner from a renewable energy source, such as solar energy.[1] Unlike the electricity produced from the most common photovoltaic cells, hydrogen could store the solar energy in the form of chemical energy. One of the most attractive solar energy conversion reactions is the photoelectrochemical (PEC) or photocatalytic water splitting directly to H_2 and O_2. Since its initial demonstration by Fujishima and Honda with a TiO_2 electrode under ultraviolet light,[2] there has been steady progress in this field in search of semiconductor photocatalytic electrode materials that work under visible light irradiation for ample solar light absorption. However, the photocatalysts with high efficiency, durability, and economic feasibility are still elusive.[3,4]

Scheelite-monoclinic $BiVO_4$ ($m$$BiVO_4$) is a well-known photocatalyst, which absorbs visible light owing to a suitable band-gap energy ($E_g \approx 2.4$ eV).[5,6] It is also nontoxic and chemically stable in aqueous solution under irradiation. However, pristine $m$$BiVO_4$ usually shows a low photocatalytic activity owing to poor charge-transport characteristics[7] and the weak surface adsorption properties.[8] Numerous attempts have been made to improve the photocatalytic activity of $BiVO_4$, including heterojunction structure formation,[7,9,10] loading co-catalysts,[11–13] and impurity doping.[8,14,15]

Impurity doping, that is, the addition of a small percentage of foreign atoms in the regular crystal lattice of semiconductors, produces dramatic changes in their electrical properties by increasing their electron or hole densities. In photocatalysis by $BiVO_4$, for example, doping with molybdenum to replace a small fraction of vanadium was found to improve the photocatalytic activity for water oxidation.[8,14,15] Phosphorus is a typical dopant for silicon or germanium to make it an n-type semiconductor. However, it has been rarely used as dopant for semiconductor photocatalysts. This is rather surprising because other non-metallic elements, such as N, C, and S, have been widely used as anionic dopants for photocatalysts to reduce their band-gap energies.[16]

In the present work, for the first time we doped phosphorous into the vanadium sites in the host lattice of $BiVO_4$, replacing some of the VO_4 oxoanions in $BiVO_4$ with PO_4 oxoanions. Oxoanion doping into the photocatalyst is to the best of our knowledge also a new concept. Herein we report effects of PO_4 oxoanion doping on the photoelectrochemical or photocatalytic behavior of $m$$BiVO_4$ under visible-light illumination. The PO_4 oxoanion doping did not bring about significant changes in the optical absorption behavior and crystal structure of $m$$BiVO_4$. When an appropriate amount PO_4 oxoanion was doped, however, the activity of photoelectrochemical water oxidation increased very significantly by a factor of about 30. The origin of the enhanced photoelectrochemical properties of PO_4 oxoanion-doped $BiVO_4$ was elucidated by using electrochemical impedence spectroscopy (EIS) and density functional theory (DFT) calculations.

The XRD patterns of pristine $BiVO_4$ and three PO_4-doped $BiVO_4$ samples with different target atom ratios (0.5%, 1%, and 5%) are shown in Figure 1a. These four patterns are identical to that of pure monoclinic $BiVO_4$ (clinobisvanite; space group: $I2/a$, JCPDS card No. 014-0688) without any impurity phase, such as $BiPO_4$ and oxides of bismuth or vanadium. Figure 1b exhibits the magnified view of (121) and (040) peaks, which show gradual shifts of peaks toward lower angles with increasing PO_4 oxoanion doping level. The 5% PO_4-doped sample shows the largest peak shift by 0.10°. The full-width at half-maximum (FWHM) also gradually increases by 11% compared with pristine $BiVO_4$, reflecting the increased strain or reduced grain size of the doped photocatalyst. These XRD results indicate that P^{5+} has been well inserted into V^{5+} sites of the host $BiVO_4$ lattice without forming any segregated impurity phase.[17]

The UV/Vis absorption spectra of the pristine and three doped $BiVO_4$ samples are illustrated in Figure 1c. The shape of the UV/Vis absorption spectra of the four samples are almost the same despite PO_4 doping. The optical band-gap energies of the four samples were estimated from the absorption spectra by using the following relationship: $\alpha h\nu = A(h\nu - E_g)^{n/2}$ where α, $h\nu$, A, and E_g are the absorption coefficient, the photon energy, constant, and the optical band-

[*] W. J. Jo,[+] Dr. J.-W. Jang,[+] H. J. Kang, J. Y. Kim, Dr. H. Jun, Dr. K. P. S. Parmar, Prof. J. S. Lee
Department of Chemical Engineering and Division of Advanced Nuclear Engineering, Pohang University of Science and Technology (POSTECH)
San 31, Hyoja-dong, Pohang 790-784 (Korea)
E-mail: jlee@postech.ac.kr
Dr. K.-j. Kong
Korea Institute of Chemical Technology
100 Jang-dong, Yuseong-gu, Daejeon, 305-343 (Korea)
[+] These authors contributed equally to this work.

[**] This research was supported by thr Hydrogen Energy Centre (a Frontier Research Program of NRF, Korea), the Korean Centre for Artificial Photosynthesis (NRF-2011-C1AAA001-2011-0030278), WCU, Brain Korea 21, and A3 foresight programs (NRF, Korea).

Supporting information for this article is available on the WWW under http://dx.doi.org/10.1002/anie.201108276.

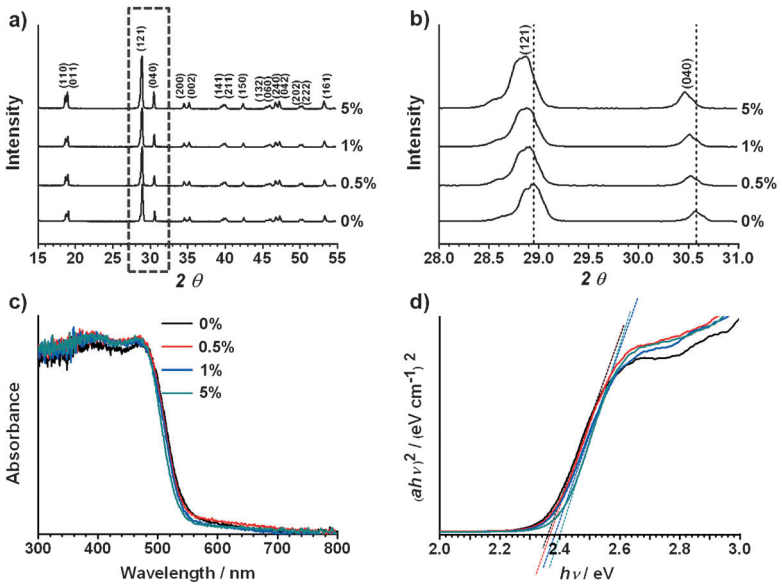

Figure 1. a) X-ray diffraction of pristine $BiVO_4$, and 0.5%, 1%, and 5% PO_4-doped $BiVO_4$; b) magnified peaks of (120) and (040) planes. c) UV/Vis absorption spectra and d) Tauc plot of bare $BiVO_4$, and 0.5, 1, and 5% PO_4-doped $BiVO_4$.

gap energy, respectively. The value of n depends on whether the transition is direct ($n=1$) or indirect ($n=4$), and it was determined to be unity from the absorption spectra. The band-gap energy was determined by extrapolating the linear part of $(\alpha h\nu)^2$ vs. $h\nu$ plot to the energy axis at $a=0$ as shown in the Figure 1 d. According to the Tauc plot, the optical band-gap energies of the four samples are not much different, yet they showed systematic increase with P doping level, that is, pristine $BiVO_4$ (ca. 2.36 eV), 0.5% P (ca. 2.37 eV), 1% P (ca. 2.38 eV), and 5% P (ca. 2.40 eV). The small difference in band gap will be discussed based on the results of DFT calculations.

The morphology and microstructure of the pristine and PO_4-doped samples observed by FESEM are exhibited in Figure S1 of Supporting Information. The close inspection of the images reveals that the particle shape of the four samples is an irregular polyhedron and the morphology and size distribution of 0.5, 1% PO_4-doped $BiVO_4$ were similar to those of pristine $BiVO_4$. However, for 5% PO_4-doped $BiVO_4$, average size of $BiVO_4$ particles was much smaller than that of pristine $BiVO_4$ (Supporting Information, Figure S1 d inset). When a large amount of PO_4 is doped into the lattice of $BiVO_4$, it seems to interfere with the crystallization of $BiVO_4$, making average size of $BiVO_4$ smaller. This is also consistent with the increased FWHM of (121) and (040) peaks for the heavily doped sample.

The real atomic ratios of vanadium to phosphorus of the three PO_4-doped $BiVO_4$ samples were determined by the ICP analysis. Table S1 of Supporting Information indicates that the actual concentrations of vanadium of the three samples are less than those introduced initially during the synthesis. It appears that the PO_4 oxoanion not doped into the $BiVO_4$ lattice has been dissolved in water and removed during the purification step.

It is possible that the PO_4 anion is present as $BiPO_4$ forming a heterojunction with $BiVO_4$ instead of doping into the $BiVO_4$ lattice. To check the existence of $BiPO_4$, we performed SEM-EDS point analysis several times, especially on the small particles scattered over the surface of a large $BiVO_4$ particle (Supporting Information, Figure S1). The concentration of phosphorus in 0.5% and 1% PO_4-doped $BiVO_4$ was below the detection limit of SEM-EDS, yet phosphorous contents in 5% PO_4-doped $BiVO_4$ (3.5%) was comparable with the actual doping amount (Supporting Information, Figure S2). This indicates that many small particles on the surface of a large $BiVO_4$ particle are not $BiPO_4$ but PO_4-doped $BiVO_4$.

To further investigate the state of the PO_4 doping, HR-TEM EDS elemental mapping was carried out. Figure 2 a shows a high-angle annular dark-field (HAADF) image of a 0.5% PO_4-doped $BiVO_4$ particle. The EDS elemental maps in Figure 2 b–e demonstrate that Bi, V, P, and O are distributed homogeneously within the 0.5% PO_4-doped $BiVO_4$ particle. The homogeneous distribution of the four elements were also confirmed in 1% and 5% PO_4-doped samples (Supporting Information, Figure S3, S4). These results show that the PO_4 oxoanion has been doped into the $BiVO_4$ lattice well without producing any segregated-phase-like vanadate, bismuth oxides, or $BiPO_4$. Figure 2 f shows a lattice spacing of 0.312 nm corresponding to the interplanar spacing of (130) plane of $m$$BiVO_4$.

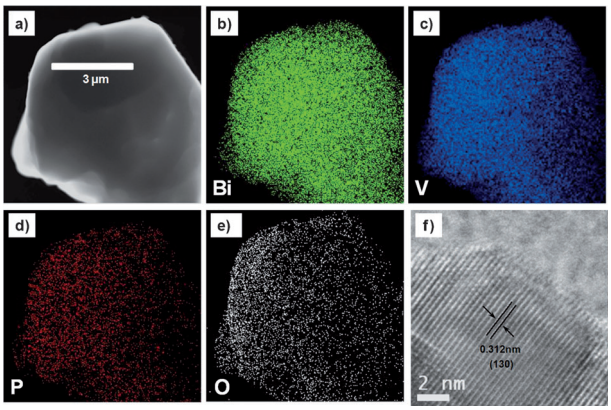

Figure 2. a) High-angle annular dark-field (HAADF) image of a 0.5% PO_4-doped $BiVO_4$ particle. b)–e) Elemental mapping of b) Bi, c) V, d) P, and e) O. f) HR-TEM image of the doped particle showing the interplanar spacing of (130) plane of monoclinic $BiVO_4$ (0.312 nm).

Photocurrent density accompanying water oxidation was measured to elucidate the effect of PO_4 doping into the $m$$BiVO_4$ lattice under visible light ($\lambda \geq 420$ nm). All the samples were synthesized in a powder form by urea-precipitation method and they were loaded onto the fluorine-doped tin oxide (FTO) glass by using electrophoretic deposition (EPD) technique. Figure 3 a illustrates how photocurrent

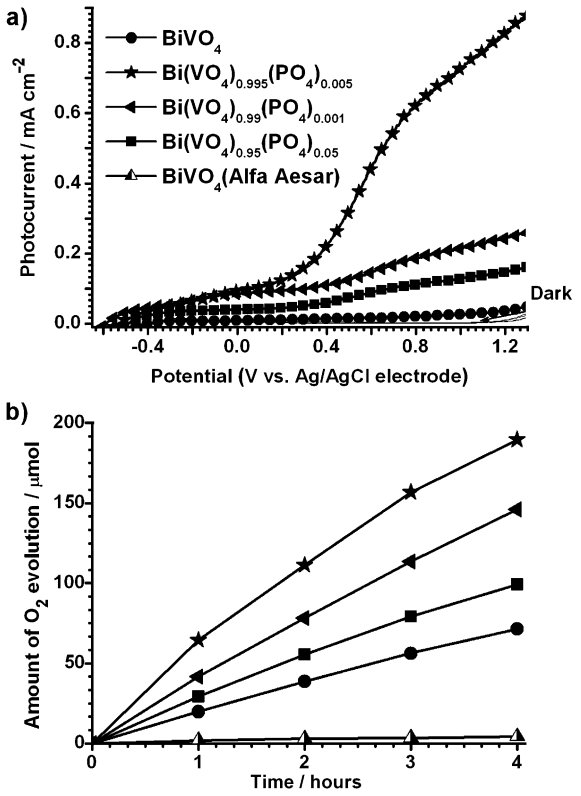

Figure 3. a) Photocurrent–potential curves of pristine $BiVO_4$, and 0.5, 1, and 5% PO_4-doped $BiVO_4$. The back side of photo-anodes was illuminated with a xenon arc lamp (300 W) fitted with a UV cut-off filter ($\lambda \geq 420$ nm). b) Photocatalytic water oxidation with bare and PO_4-doped $BiVO_4$ under the visible-light ($\lambda > 420$ nm) irradiation. The photocatalyst powders (0.1 g) were dispersed in aqueous $AgNO_3$ solution as an electron scavenger.

density of the four photoanodes varies under dark and visible light illumination as applied anodic potential increases from -0.6 V to $+1.2$ V (vs. Ag/AgCl). Visible light irradiation on photoanodes drives PEC water oxidation reactions to generate photoelectrons, which are collected by the FTO substrate to produce currents: $2H_2O(l) + h\nu \rightarrow O_2(g) + 4H^+ + 4e^-$.

As Figure 3a shows, the photocurrent increased dramatically by PO_4 oxoanion doping. In the best case, the photocurrent (0.548 mA cm^{-2} at 0.7 V) produced by 0.5% PO_4-doped $BiVO_4$ is about 30 times higher than the photocurrent (0.019 mA cm^{-2} at 0.7 V) produced by pristine $BiVO_4$. The potential (0.7 V) adopted for comparison corresponds to 1.23 V vs. RHE at pH 6.6, which is the theoretical potential necessary for water oxidation: $E_{RHE} = E_{Ag/AgCl} + 0.059\ pH + E^\circ_{Ag/AgCl}$ ($E^\circ_{Ag/AgCl} = 0.209$ V at 25 °C) The 1% and 5% PO_4-doped $BiVO_4$ anodes also showed much enhanced photocurrents relative to the pristine $BiVO_4$ electrode, but they were much less than that for 0.5% PO_4-doped $BiVO_4$.

The photocatalytic water oxidation activity of pristine and PO_4-doped $BiVO_4$ photocataltysts were also measured for powder samples in 100 mL of aqueous $AgNO_3$ solution under visible light irradiation ($\lambda > 420$ nm). Here, Ag^+ ions from $AgNO_3$ played the role of an electron scavenger: $2H_2O(l) + h\nu \rightarrow O_2(g) + 4H^+ + 4Ag$. In line with the trend of photocurrent generation shown in Figure 3a, Figure 3b shows that the largest amount of O_2 is evolved by 0.5% PO_4-doped $BiVO_4$, which is more than triple the amount of O_2 evolved by bare $BiVO_4$. The order of activity was also the same: pristine $BiVO_4$ < 5% PO_4-doped < 1% PO_4-doped < 0.5% PO_4-doped $BiVO_4$. It should also be noted that the photocatalytic activities of the four $BiVO_4$ samples prepared by the urea-precipitation method are much higher than the commercial $BiVO_4$ (Alfa Aesar, 99.9%).

To study the origin of the enhanced PEC and photocatalytic activity, electrochemical behavior of PO_4-doped $BiVO_4$ was investigated by the electrochemical impedance spectroscopy (EIS).[18] The EIS measurements were carried out at the same condition where semiconductor generated photocurrents (0.7 V vs. Ag/AgCl, visible light) to relate the impedance response directly to the physical processes responsible for the photocurrent generation.[19] The results of EIS are presented in Figure 4 in the form of Nyquist plots. Here,

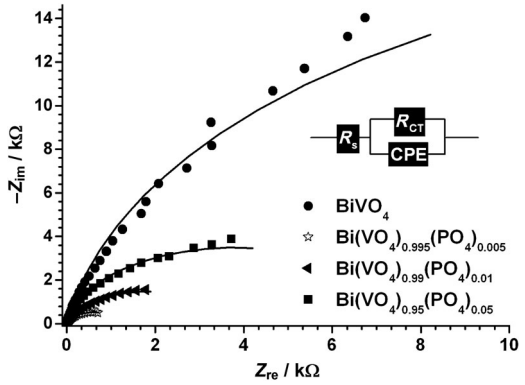

Figure 4. Electrochemical impedence spectroscopy measured at 0.7 V (vs. Ag/AgCl) in 0.5 M Na_2SO_4 solution. The inset shows an equivalent circuit for the photoanodes (see text for details).

the x axis represents the real part of measured impedance and the y axis represents the negative number of the imaginary part of measured impedance. The small dots in the plot represent the experimental data and the solid lines represent the result of fitting these experimental data to the equivalent circuit model. The solid line was fitted by ZSimpWin software using the proposed equivalent circuit model. The Nyquist plot can be interpreted in terms of the equivalent circuit as displayed in the inset. Here, the EIS data were measured using a three-electrode cell system, thus the arc in Nyquist plot represents the charge transfer kinetics on the working electrode. We selected the Randles-Ershler model,[20] in which R_s is the solution resistance, CPE is the capacitance phase element for the semiconductor||electrolyte interface, and R_{ct} is the charge transfer resistance across the interface. The smaller value of R_{ct} and the larger value of a CPE represent improved charge transport characteristics making favorable environment for charge separation in PEC reactions. An RC circuit represents an interface within the cell. Thus, the arcs in the Nyquist plot are related to charge transfer at the semiconductor||electrolyte interface.

The fitted values of R_{ct} were 36946, 1206, 3685, and 7651 Ω for pristine $BiVO_4$, 0.5%, 1%, and 5% PO_4-doped $BiVO_4$ electrodes, respectively. The fitted value of R_{ct} for 0.5% PO_4-doped $BiVO_4$ is about 30 times smaller than that of pristine $BiVO_4$, which show a perfect correlation with the activity trends of both PEC photocurrent generation and photocatalytic O_2 generation. Thus, the improved charge transfer characteristic of PO_4-doped $BiVO_4$ is the most important factor responsible for their enhanced photocatalytic performance. The efficient charge transfer at the semiconductor||electrolyte interface suppresses the charge recombination and enhance the efficiency of PEC water oxidation.[7,21] When the PO_4 doping level increased to 1% or 5%, charge transfer resistance increased compared with 0.5%-doped $BiVO_4$. The excessive amount of PO_4 oxoanion doping seems to form defect sites in the monoclinic $BiVO_4$ lattice, which act as electron–hole recombination sites.

By unprecedented PO_4 oxoanion doping of *m*$BiVO_4$, we observed a dramatic enhancement of photoelectrochemical water oxidation activity by a factor of about 30. According to the EIS study, this is correlated well with the greatly improved change transfer characteristics at the semiconductor||electrolyte interface. To elucidate the pronounced doping effect, we performed density functional theory (DFT) calculations of electronic structures.

Clinobisvanite $BiVO_4$ has a monoclinic structure (point group: C^6_{2h}, space group: *C2/c*) and contains four bismuth or vanadium atoms and sixteen oxygen atoms in the unit cell. Its basic structural unit is constructed by VO_4 tetrahedron and BiO_8 dodecahedron, in which bismuth and vanadium atoms are arranged alternately to form a continuous zigzag line on the $(22\bar{1})$ plane. To obtain self-consistent results, we optimized lattice constants and atomic coordinates, which were obtained by minimizing the total energy, internal stress, and atomic forces. This was done by performing an iterative process in which the cell parameters and coordinates of the atoms are adjusted so that the total energy of the structure is minimized. The relaxation run was considered converged when the force on the atom was less than 0.01 eV Å^{-1}. By doing so, we could obtain stable structures for all of the models. By optimizing the pure clinobisvanite $BiVO_4$ structure, we obtained the lattice parameters as follows: $a = 7.304$, $b = 11.744$, $c = 5.165$ Å, $\beta = 135.003°$. These parameters were in good agreement with experimental values:[22] $a = 7.258$, $b = 11.706$, $c = 5.084$ Å, $\beta = 134.073°$. Because doping occurs within bulk $BiVO_4$, our PO_4 doping model uses the same lattice constants with pristine $BiVO_4$. To avoid the self-interactions of impurity, we adopted the supercell method with sufficient length on all directions. Our PO_4 doping model consists of two unit cells stacked both along the *a* and *c* axes in which one of sixteen vanadium atoms is substituted by a phosphorus atom (6.25% of PO_4 doped), which is comparable to those used in the experiments.

Figure 5a shows the projected density of states (pDOS) of pristine $BiVO_4$ and P-doped $BiVO_4$. The calculated band gap of pure $BiVO_4$ is about 1.94 eV, which is smaller than the experimental value of 2.36 eV owing to the well-known limitation of DFT, that is, the underestimation of band gap. Upon PO_4 doping, the band gap becomes slightly larger

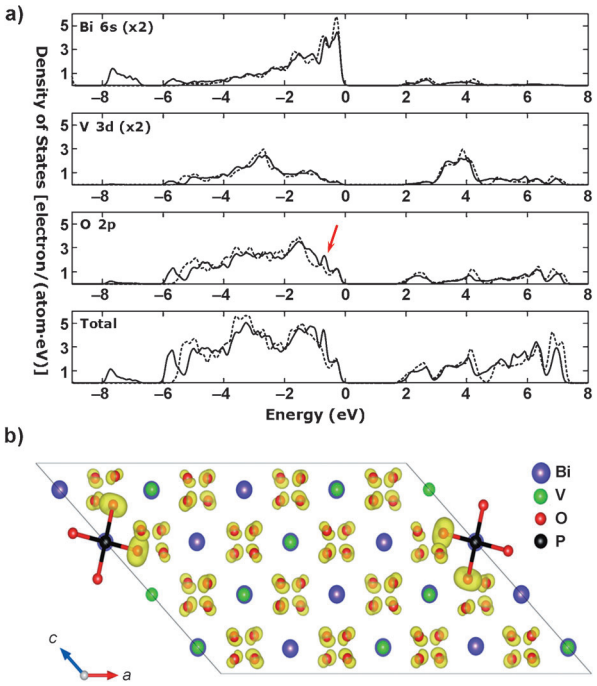

Figure 5. a) Total and local partial density of states of monoclinic clinobisvanite $BiVO_4$ (••••) and P-doped $BiVO_4$ (——). The main effect of P-doping occurs as an additional O2p peak at −0.7 eV (marked by an arrow). The DOS is decomposed into the main electron states of each component. Note the slight increase of band gap upon P substitution. b) Calculated isosurface (0.04 el Å^{-1}) of integrated charge density in the range from −0.7 eV to E_f for P-doped $BiVO_4$. Note the enhancement of p_π states of O bonded with the P atom. Only P–O bonds are shown for clarity.

(1.95 eV for 6.25% doping and 2.00 eV for 25%). This result corrsponds well with a slight band-gap change obtained by the Tauc plots. This is also one of the important pieces of evidence that the PO_4 oxoanion is well-doped.

As is well-known for metal oxides, the top of valence band (VB) is composed of O2p states and conduction band (CB) bottom comes from V3d states. Upon PO_4 substitution, the DOS of the VB top increases; the ratio of integrated DOS in the energy windows of −0.7 eV from the VB top to total electrons is 4.0% and 5.9% for pristine and PO_4-doped $BiVO_4$, respectively. The larger DOS in the VB around the Fermi energy E_F implies an increase of charge carriers, resulting in lower R_{CT}. This will lead to higher PEC activity.

The Bader charge analysis[23] shown in Figure 5b suggests that the substituted phosphorus atom has a much smaller charge (1.357 electrons) than the vanadium atoms (3.102 electrons). The depleted electrons from the phosphorus atom accumulate around neighboring oxygen atoms, enhancing the non-bonding O2p_π states. The calculated Bader charges of oxygen atoms in the PO_4 tetrahedron slightly fluctuate in the range from 7.406 to 7.453 electrons. The oxygen atoms have charges of 6.966 electrons in the pristine $BiVO_4$. The length of the P–O bond is 1.563 Å, which is slightly smaller than the V–O bond (1.737 Å). Owing to the lattice strain imposed by the different V–O and P–O bond lengths and the charge redistribution around the dopant, there exists an internal

electric field. This effect is very advantageous for the separation of electron–hole pairs, which can improve the photocatalytic property.

To summarize, we have investigated PO_4 oxoanion doping into *m*$BiVO_4$ for the first time. The 0.5 % PO_4-doped $BiVO_4$ showed the best photocurrent density, which is about 30 times higher than that of pristine $BiVO_4$. The same trend was observed for photocatalytic O_2 evolution rates. EIS measurements revealed that PO_4 oxoanion doping lowered the charge transfer resistance of *m*$BiVO_4$ remarkably. Finally, DFT calculations showed increased charge carriers in PO_4-doped *m*$BiVO_4$. Both results indicate that the origin of the enhanced photoelectrochemical and photocatalytic properties of PO_4 oxoanion-doped *m*$BiVO_4$ greatly improves the charge-transfer characteristics of *m*$BiVO_4$.

Received: November 24, 2011
Published online: February 17, 2012

Keywords: bismuth · doping · phosphates · photolysis · vanadates

[1] M. Grätzel, *Inorg. Chem.* **2005**, *44*, 6841 – 6851.
[2] A. Fujishima, K. Honda, *Nature* **1972**, *238*, 37 – 38.
[3] K. Maeda, K. Domen, *J. Phys. Chem. C* **2007**, *111*, 7851 – 7861.
[4] D. Yamasita, T. Takata, M. Hara, J. N. Kondo, K. Domen, *Solid State Ionics* **2004**, *172*, 591 – 595.
[5] A. Kudo, K. Omori, H. Kato, *J. Am. Chem. Soc.* **1999**, *121*, 11459 – 11467.
[6] S. Tokunaga, H. Kato, A. Kudo, *Chem. Mater.* **2001**, *13*, 4624 – 4628.
[7] S. J. Hong, S. Lee, J. S. Jang, J. S. Lee, *Energy Environ. Sci.* **2011**, *4*, 1781 – 1787.
[8] W. Yao, H. Iwai, J. Ye, *Dalton Trans.* **2008**, 1426 – 1430.
[9] M. Long, W. Cai, H. Kisch, *J. Phys. Chem. C* **2008**, *112*, 548 – 554.
[10] H. Q. Jiang, H. Endo, H. Natori, M. Nagai, K. Kobayashi, *Mater. Res. Bull.* **2009**, *44*, 700 – 706.
[11] H. Xu, H. Li, C. Wu, J. Chu, Y. Yan, H. Shu, Z. Gu, *J. Hazard. Mater.* **2008**, *153*, 877 – 884.
[12] S. Kohtani, M. Tomohiro, K. Tokumura, R, Nakagaki, *Appl. Catal. B* **2005**, *58*, 265 – 272.
[13] S. Kohtani, J. Hiro, N. Yamamoto, A. Kudo, K. Tokumura, R. Nakagaki, *Catal. Commun.* **2005**, *6*, 185 – 189.
[14] W. Yao, J. Ye, *J. Phys. Chem. B* **2006**, *110*, 11188 – 11195.
[15] W. Luo, Z. Yang, Z. Li, J. Zhang, J. Liu, Z. Zhao, Z. Wang, S. Yan, T. Yu, Z. Zou, *Energy Environ. Sci.* **2011**, *4*, 4046 – 4051.
[16] R. Asahi, T. Morikawa, T. Ohwaki, K. Aoki, Y. Taga, *Science* **2001**, *293*, 269 – 271.
[17] A. Zhang, J, Zhang, *J. Hazard. Mater.* **2010**, *173*, 265 – 272.
[18] S. Banerjee, S. K. Mohapatra, P. P. Das, M. Misra, *Chem. Mater.* **2008**, *20*, 6784 – 6791.
[19] E. A. Ponomarev, L. M. Peter, *J. Electroanal. Chem.* **1995**, *396*, 219 – 226.
[20] J. E. Randles, *Discuss. Faraday Soc.* **1947**, *1*, 11 – 19.
[21] X. M. Song, J. M. Wu, M. Z. Tang, B. Qi, M. Yan, *J. Phys. Chem. C* **2008**, *112*, 19484 – 19492.
[22] A. W. Sleight, H. y. Chen, A. Ferretti, D. E. Cox, *Mater. Res. Bull.* **1979**, *14*, 1571 – 1581.
[23] G. Henkelman, A. Arnaldsson, H. Jónsson, *Comput. Mater. Sci.* **2006**, *36*, 354 – 360.

